Materials Science Forum
ISSN: 1662-9752, Vol. 1188, pp 107-116
doi:10.4028/p-u66D1M
© 2026 The Author(s). Published by Trans Tech Publications Ltd, Switzerland.
Submitted: 2026-02-13
Revised: 2026-02-19
Accepted: 2026-02-22
Online: 2026-04-20

Numerical and Experimental Design of a Step HPDC Mould for Process-Microstructure Correlation in Lightweight Component

Alessandro MORRI[1, a], Barbara REGGIANI[2,3, b], Rosario SQUATRITO[2,c]
Manel da Silva[4,d], Giulia ZANIBONI[2,e*], Lorenzo DONATI[1,f]

[1]Department of Industrial Engineering, University of Bologna, Viale Risorgimento 2, 40133 Bologna, Italy

[2]Department of Science and Method for Engineering, University of Modena and Reggio Emilia, Via Amendola 2, 42122 Reggio Emilia, Italy

[3]INTERMECH, University of Modena and Reggio Emilia, Via Amendola 2, 42122, Italy

[4]Eurecat, Centre Tecnològic de Catalunya, Unit of Metallic and Ceramic Materials, Av. Universitat Autònoma 23, 08290 Cerdanyola del Vallès, Barcelona, Spain

[a]alessandro.morri4@unibo.it, [b]barbara.reggiani@unimore.it, [c]rosario.squatrito@unimore.it,

[d]manel.dasilva@eurecat.org, [e]giulia.zaniboni@unimore.it*, [f]l.donati@unibo.it

Keywords: Microstructural prediction, High-pressure die casting (HPDC), step casting mould

Abstract. The increasing demand for lightweight and energy-efficient components has strengthened the use of high-pressure die casting (HPDC) for thin-walled aluminium parts, often produced from recycled alloys. However, HPDC components are still affected by microstructural heterogeneity and defect formation, such as shrinkage porosity and gas entrapment, which are closely related to melt flow and solidification conditions. In this study, a dedicated step-casting geometry was developed to reproduce, within a single casting, solidification conditions representative of industrial HPDC components with varying thickness. The design was supported by numerical simulations to control filling and thermal evolution. Experimental HPDC trials were performed under industrial conditions, followed by microstructural characterization in terms of porosity, Secondary Dendrite Arm Spacing (SDAS) and skin layer thickness. Comparison with a complex industrial demonstrator component confirmed that the step casting reliably reproduces both average microstructural features and their variability. The proposed numerical–experimental approach provides a robust framework for process HPDC design and optimization for lightweight cast components.

Introduction

The increasing industrial focus on energy efficiency and environmental sustainability has made the production of lightweight metal components a strategic priority across several application fields, particularly in the transportation and automotive sectors [1]. In this context, aluminium alloys, often derived from recycled feedstock, offer an attractive combination of low density, good mechanical performance and reduced environmental footprint.

High-pressure die casting (HPDC) is widely adopted for the manufacturing of lightweight aluminium components due to its capability to produce complex geometries with thin walls, high dimensional accuracy and short cycle times [2], [3], [4]. Despite its technological maturity and extensive industrial use, HPDC still poses significant challenges in terms of controlling microstructural evolution and defect formation during solidification [5]. The extreme process conditions characterizing HPDC, like high filling velocities and compacting pressures, rapid heat extraction and complex thermal gradients, make the final microstructure highly sensitive to local process variations.

Small changes in melt temperature, cooling rate or metal flow behaviour can significantly alter key microstructural features such as porosity distribution, dendritic morphology and skin layer development, ultimately affecting the mechanical strength, ductility and fatigue resistance of the final component [6], [7]. In particular, turbulence during cavity filling plays a critical role in promoting

This article is an open access article under the terms and conditions of the Creative Commons Attribution (CC BY) license (https://creativecommons.org/licenses/by/4.0)

gas entrapment and oxide formation, while insufficient feeding during solidification leads to shrinkage porosity, especially in thicker sections. These phenomena are often strongly coupled and difficult to mitigate simultaneously in industrial-scale components.

Numerical simulations have therefore become an essential tool for the analysis and optimization of HPDC processes. Modern simulation frameworks allow the investigation of mould filling dynamics, temperature evolution, cooling rates and solidification times prior to experimental trials, significantly reducing development time and costs. However, simulation alone is not sufficient to fully describe the complex thermo-fluid and metallurgical phenomena occurring during HPDC [8]. The predictive capability of numerical models strongly depends on reliable experimental validation, particularly with respect to microstructural features and defect formation mechanisms.

Industrial HPDC components are typically characterized by large thickness variations, local hot spots and intricate internal cavities, which make it difficult to isolate the specific process parameters governing microstructural evolution. As a result, there is growing interest in the development of controlled casting geometries that can reproduce, in a simplified and repeatable manner, the thermal and solidification conditions encountered in real components, while remaining sufficiently simple to allow systematic investigation.

Among the proposed solutions, step casting geometries represent an effective experimental approach, as they enable the generation of distinct solidification regimes within a single casting by varying wall thickness and local heat extraction conditions. When combined with validated numerical simulations, step castings provide a robust platform for studying the relationships between process parameters, microstructural features, such as Secondary Dendrite Arm Spacing (SDAS), porosity content and skin layer thickness, and the resulting mechanical performance [9].

In this work, a dedicated step casting was designed and optimized through numerical simulations with the objective of minimizing turbulence-induced defects and shrinkage porosity while reproducing microstructural conditions representative of industrial HPDC components. After the optimization, the casting was produced under controlled industrial HPDC conditions and extensively characterized from a microstructural standpoint. A direct comparison with a complex industrial demonstrator component was carried out to validate the representativeness of the step casting, establishing a solid foundation for future process–microstructure–property correlations and data-driven modelling strategies for lightweight aluminium HPDC components.

Step Casting Design and Optimization

The mould used for the experimental production of the components was created following an assessment using numerical simulations, which made it possible to identify the critical points of the geometry and optimize it.

The base mould (M0) of the step component was available at the Eurecat industrial facilities (Cerdanyola del Vallès, Barcelona). The step casting component obtained from the M0 had a step-shaped geometry thought reproduce, within a single HPDC component, a significant range of solidification and cooling conditions representative of industrial lightweight parts. The specimen consisted of a plate 170 mm in width and 180 mm in height, composed of six steps with decreasing thickness, ranging from 15 mm to 1 mm. Each step had a height of 29 mm, except for the thickest one, which was 23 mm. The ingate was dimensioned as 67 mm in width and 4mm in height, for a total feeding area of 267 mm^2, and positioned in correspondence with the thickest step to promote efficient feeding. Vents were placed near the thinnest sections to facilitate air evacuation during filling (Figure 1a).

For the numerical simulations, ProCAST 2025 was employed using a simplified representation of the die in order to reduce computational time. Since the primary objective of the simulations was the comparative evaluation of the step casting geometry, all analyses were performed using the aluminium alloy EN AC43500 selected from the ProCAST material database. As illustrated in the Figure 1b, the die casting system was simplified by explicitly modelling only the mould components directly in contact with the molten alloy of the component, namely the cavity insert and the gating system. In addition, the mould holder was included in the numerical model to account for the global

thermal inertia of the die assembly. This modelling strategy allows a significant reduction in computational cost while preserving the predictive capability of the simulation, particularly with respect to the thermal behaviour of the mould and its influence on filling dynamics, solidification and shrinkage porosity formation.

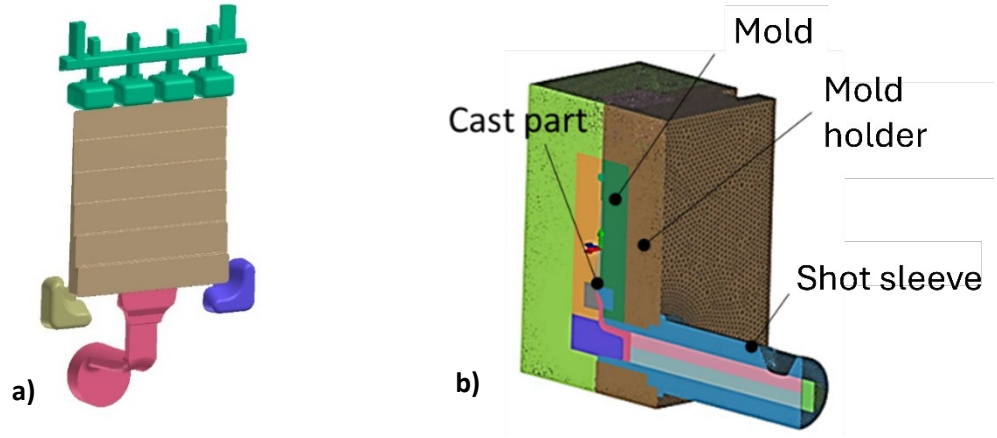


Fig. 1. a) Base step casting geometry, b) solid model used to perform the simulation

The simulation parameters were set in accordance with previous experimental data obtained at Eurecat [10], ensuring consistency with industrial HPDC operating conditions. In particular, the most relevant parameters for the numerical modelling of the HPDC process in ProCAST included the thermophysical properties of the alloy (density, thermal conductivity, specific heat and latent heat of solidification), as provided by the EN AC-43500 material database.

To ensure a correct evaluation, the properties of the alloy were calculated using the ProCAST tool Computherm. Starting from the alloy's chemical composition, this module extracts the phase transformation temperatures, specific heat capacity, thermal conductivity, and other thermo-physical properties crucial for simulating the casting process and predicting the final material properties

Boundary conditions at the metal–die interface were defined through heat transfer coefficients (HTC), which were assigned as a function of local contact conditions and process stage, with representative values ranging between 4000 and 10000 $W \cdot m^{-2} \cdot K^{-1}$. The evolution of HTC during the cycle was used to account for the transition from initial metal–die contact to solidification and die opening. The injection conditions were defined by imposing the piston velocity profile at the inlet, including the slow-shot and fast-shot phases, with characteristic velocities of 0.4 $m \cdot s^{-1}$ and 4 $m \cdot s^{-1}$. The melt temperature at injection and the initial die temperature were set to 680 °C and 100 °C, respectively, in agreement with the monitored industrial process conditions.

Additional modelling parameters included the filling fraction of the shot sleeve (33%), the metal fraction at the end of filling, and the criteria for shrinkage porosity prediction, based on local solidification time and feeding capability. This parameter set provided a physically consistent representation of the HPDC process and ensured reliable prediction of filling behaviour, thermal evolution and defect formation. Then, a total of 3,443,126 elements were used for the finite element mesh, consisting of hexahedral and tetrahedral elements, carefully refined in regions of high thermal gradients and complex geometry to ensure numerical accuracy. The time step for the transient simulation was set to vary over time from 0.05 to 0.1 s resulting in a total simulation duration of 81.7 s, sufficient to capture the complete filling, solidification, and ejection phases of the HPDC cycle. The analyses performed were filling and solidification, activating Thermal and Flow modules. Mesh convergence studies were performed to verify that further refinement did not significantly affect temperature, flow, or porosity predictions, thus avoiding numerical instabilities. The solver settings in ProCAST included 5 iterations per time step, with automatic stabilization routines activated to maintain convergence throughout the rapid filling phase. This setup allowed for a robust and computationally efficient simulation of the industrial HPDC process.

Concerning the achieved results, filling simulations revealed significant fluid recirculation, particularly in the thicker sections of the casting, as shown in Figure 2a. This recirculation promoted turbulent flow, increasing the risk of gas entrapment and of unwanted oxides and leading to inadequate feeding during solidification. Consistently, shrinkage porosity predictions, conducted by using the standard APM module, indicated a high concentration of defects in the thickest steps highlighting the need for geometric and process optimization (Figure 2b).

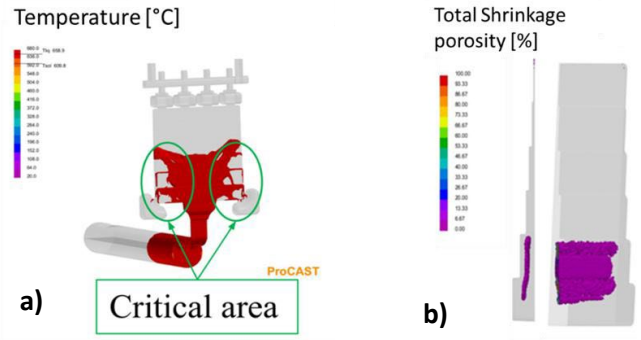


Fig. 2. Defects of the original mould design a) temperature during filling, b) total shrinkage porosity

To mitigate these issues, a multi-step redesign strategy was implemented. First, the lateral width of the steps was reduced from 170 mm to 120 mm to promote more uniform cooling and limit recirculation during filling (Figure 3a). Temperature field during the filling phase (Figure 3b) and the shrinkage porosity (Figure 3c) show a clear reduction compared to the original configuration, although some porosity remains localized in the thicker steps.

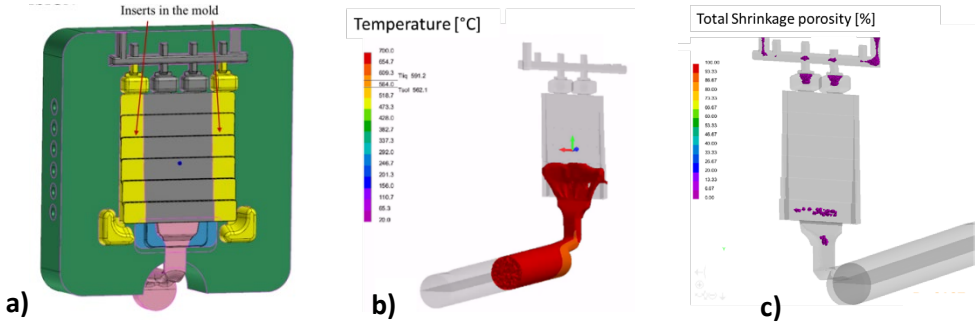


Fig. 3. a) First mould redesign, b) Temperature and c) Shrinkage porosity

This modification resulted in a clear reduction of predicted porosity, although localized shrinkage defects persisted in the thickest sections. Subsequently, further geometric refinements were introduced by increasing the ingate width to 77 mm and thickness to 6 mm to promote efficient feeding. Finally, the opposite section of the casting was chamfered with angles of 45°C (Figure 4a). The simulations of this optimized configuration show an improved feeding of the thicker step during the filling phase (Figure 4b), and the total shrinkage porosity is further reduced and significantly lower than in the original design, though not completely eliminated (Figure 4c).

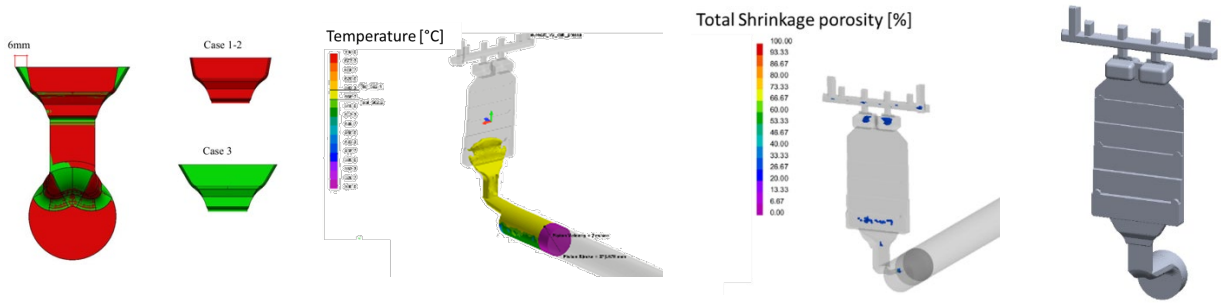


Fig. 4. a) Second mould redesign, b) Temperature and c) Shrinkage porosity, d) final Step-shaped HPDC specimen

Based on these results, this final optimized geometry was selected for casting, as it provides a good compromise between improved feeding, reduced solidification time in the thicker sections, and minimized shrinkage porosity (Figure 4d).

Step casting production

Once optimized the geometry, the step samples were casted using the aluminium alloy EN AC-43500, which nominal composition is reported in Table 1.

Table 1. Alloy composition

	Si	Fe	Mn	Mg	Zn	Ti	Cu	Cr	Sr	Al
EN 1706:2020 / EN AC-43500	9.0–11.5	<0.25	0.4–0.8	0.10–0.6	<0.07	<0.20	<0.05	<0.05	-	Bal

The step casting production was performed at the Eurecat industrial facilities (Cerdanyola del Vallès, Barcelona) using a Bühler cold chamber HPDC machine with a maximum locking force of 5250 kN, a plunger with a diameter of 60 mm and a stroke of 455 mm (Figure 5a). The plunger velocity at the filling phase was reduced from 4 m/s to 2 m/s in order to ensure a good filling of the whole part, including the section of 1 mm. The metal velocity at the ingate section was 12 m/s. The aluminium alloy was melted and held in a temperature-controlled furnace at 705 °C to ensure stable thermal conditions prior to injection. Temperature control was continuously maintained throughout the production campaign in order to guarantee process stability and repeatability. The key process parameters used both in simulation and in experimental are reported in Table2.

Table 2. Process parameters for numerical simulation and for experimental trials

Parameters	Unit	Simulation value	Experimental value
Piston velocity	$m \cdot s^{-1}$	0.4 (first phase) 4 (second phase)	0.4 (first phase) 2 (second phase)
Melt temperature	°C	680	705
Die temperature	°C	100	100
Total cycle time	S	81.7	81.7

Molten metal was injected into the die cavity following a predefined piston velocity profile, reported in Figure 5c. The injection curve describes the evolution of piston displacement and velocity during the shot cycle. A first low-speed phase was applied to enable a controlled transfer of molten metal along the shot sleeve, followed by a high-speed phase to achieve complete cavity filling before the onset of solidification. The final stage corresponds to pressure build-up and intensification, which is required to compensate for solidification shrinkage and to enhance casting soundness. The selected

injection profile is consistent with standard industrial HPDC practice for aluminium alloys and was designed to limit air entrapment while ensuring adequate filling performance.

The thermal state of the die was monitored by means of infrared temperature mapping before and after the spraying phase, as shown in Figure 5d. Three reference points were selected to track temperature evolution. The thermal images illustrate the surface temperature distribution of the die prior to lubricant application and the corresponding temperature reduction following spraying. This monitoring procedure was essential to confirm that the die operated within the desired thermal window, promoting stable solidification conditions and reducing the risk of defects related to local overheating or insufficient cooling.

The castings produced during the industrial trials consisted of the step casting components integrated with the complete feeding system. In details, the manufactured part included the step casting geometry together with the runner, runner extension, and riser (Figure 5b).

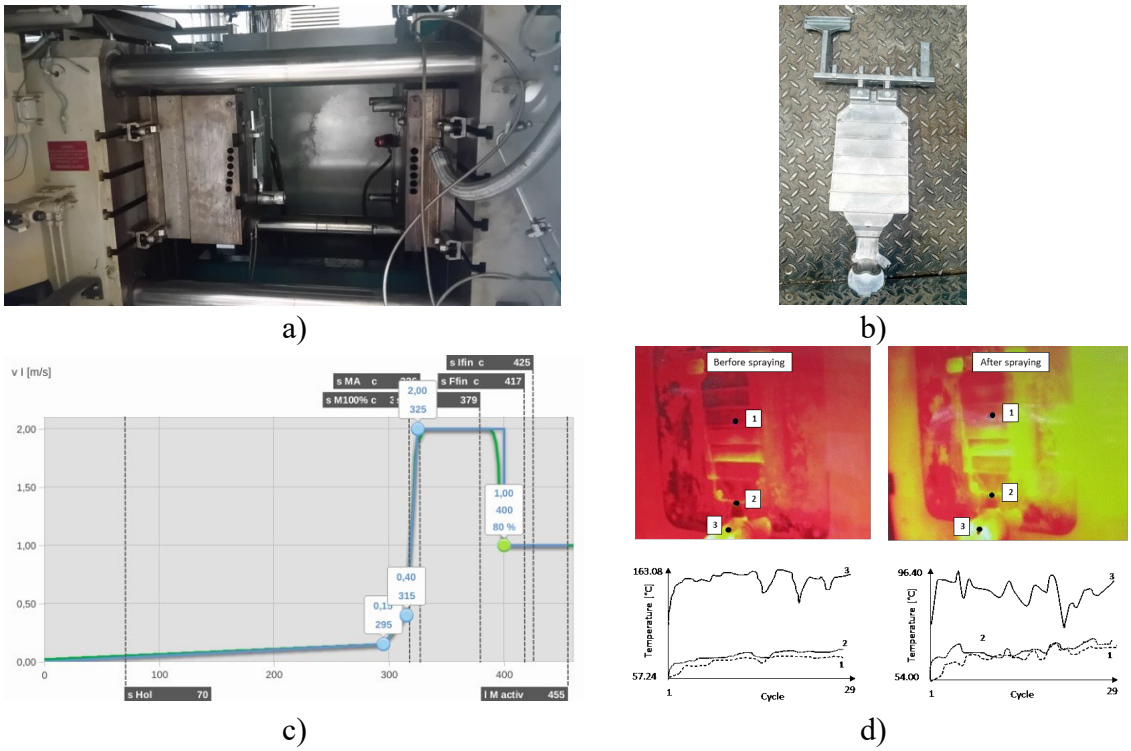
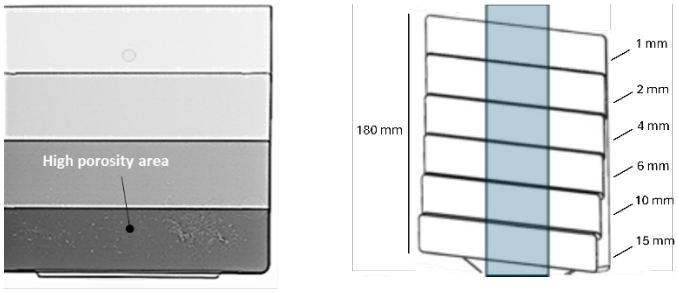


Fig. 5. a) Injection unit control interface displaying the shot sleeve configuration and filling conditions, b) final Step-shaped HPDC specimen, c) Piston injection profile (velocity over the displacement during the shot cycle) and d) Thermocamera acquisitions.

Step Casting Microstructure Investigation

Radiographic inspection and micrographs of the step castings were performed, revealing the presence of significant porosity only in the step with a thickness of 15 mm (Figure 6a). Microstructural analyses were therefore carried out in the central region of three step castings (Figure 6b), focusing on the assessment of the porosity percentage, SDAS and the thickness of the skin layer. For each step thickness the microstructural characterization was performed over the entire cross-sectional area.



a) b)

Fig. 6. (a) Radiographic inspection and microstructural analysis of a step casting, highlighting the presence of defects in selected sections; (b) Area of the step casting that underwent microstructural characterization.

As an example, Figure 7 shows the microstructures of the 2 mm and 6 mm step thicknesses. Despite the substantial variation in section thickness, only limited differences were observed in terms of porosity content and secondary dendrite arm spacing (SDAS) among the different steps.
The average porosity, assessed by metallographic analysis, ranged from 1.1% (SD 0.3%) in the 2 mm step to 1.4% (SD 0.1%) in the 6 mm step. Similarly, the SDAS varied within a narrow range, from 13 μm (SD 1.7 μm) in the 1 mm step to 14.5 μm (SD 1.0 μm) in the 15 mm step. This slight increase can reasonably be attributed to the reduction in cooling rate associated with increasing section thickness.
It should be noted, however, that the microstructure of the high-pressure die castings consists of both externally solidified crystals (ESCs), formed during the injection stage, and dendrites that developed within the die cavity. The coexistence of these distinct solidification features introduces significant heterogeneity and complicates the reliable determination of SDAS.
The skin layer thickness ranged from 35 μm (SD 19 μm) in the 1 mm step to 130 μm (SD 23 μm) in the 6 mm step. The relatively large data dispersion is mainly attributable to the discontinuous nature of the skin layer, particularly in the thinner steps, where it was not uniformly present along the entire cross-section

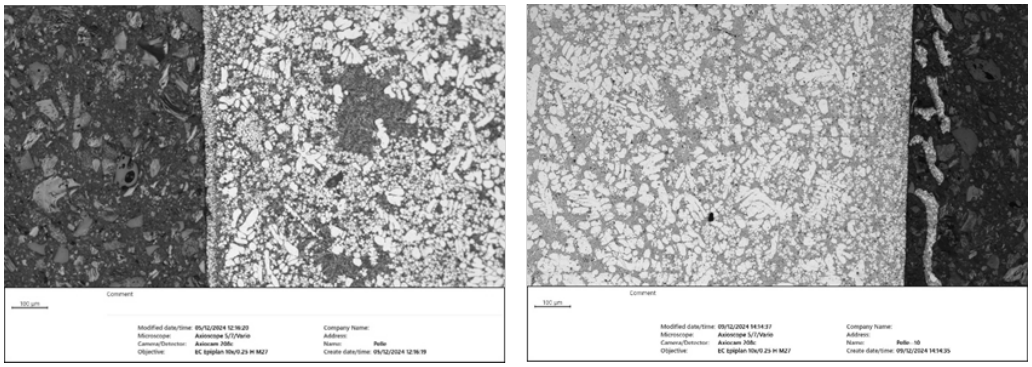


Fig. 7. Microstructure of (a) the 2 mm thickness step and (b) the 6 mm thickness step.

Industrial Component Microstructure Investigation

The selected industrial component was an engine mount manufactured by a sports car producer using the same EN AC-43500 alloy adopted for the step casting specimens and produced by a high-pressure die casting (HPDC) process assisted by squeeze pins. As in the case of the step casting samples, the microstructural analysis focused on the evaluation of porosity content, secondary dendrite arm spacing (SDAS), and skin layer thickness.
Metallographic specimens extracted from different regions of the component are shown in Figure 8a, while representative micrographs illustrating the typical microstructural features are reported in

Figures 8b and 8c. The microstructural parameters were quantified over the entire cross-sectional area of each analysed sample.
The total porosity area fraction exhibited significant variability among the different locations: a porosity level of 0.8% was measured in sample A, 1.3% in sample B, and up to 3% in sample C. Across all analysed specimens, the SDAS ranged from 14 µm (SD 2 µm) in sample A to 18 µm (SD 2 µm).
Finally, the skin layer thickness (Figure 8c) varied between a minimum of 125 µm (SD 24 µm) in sample C and a maximum of 225 µm (SD 37 µm) in sample A.

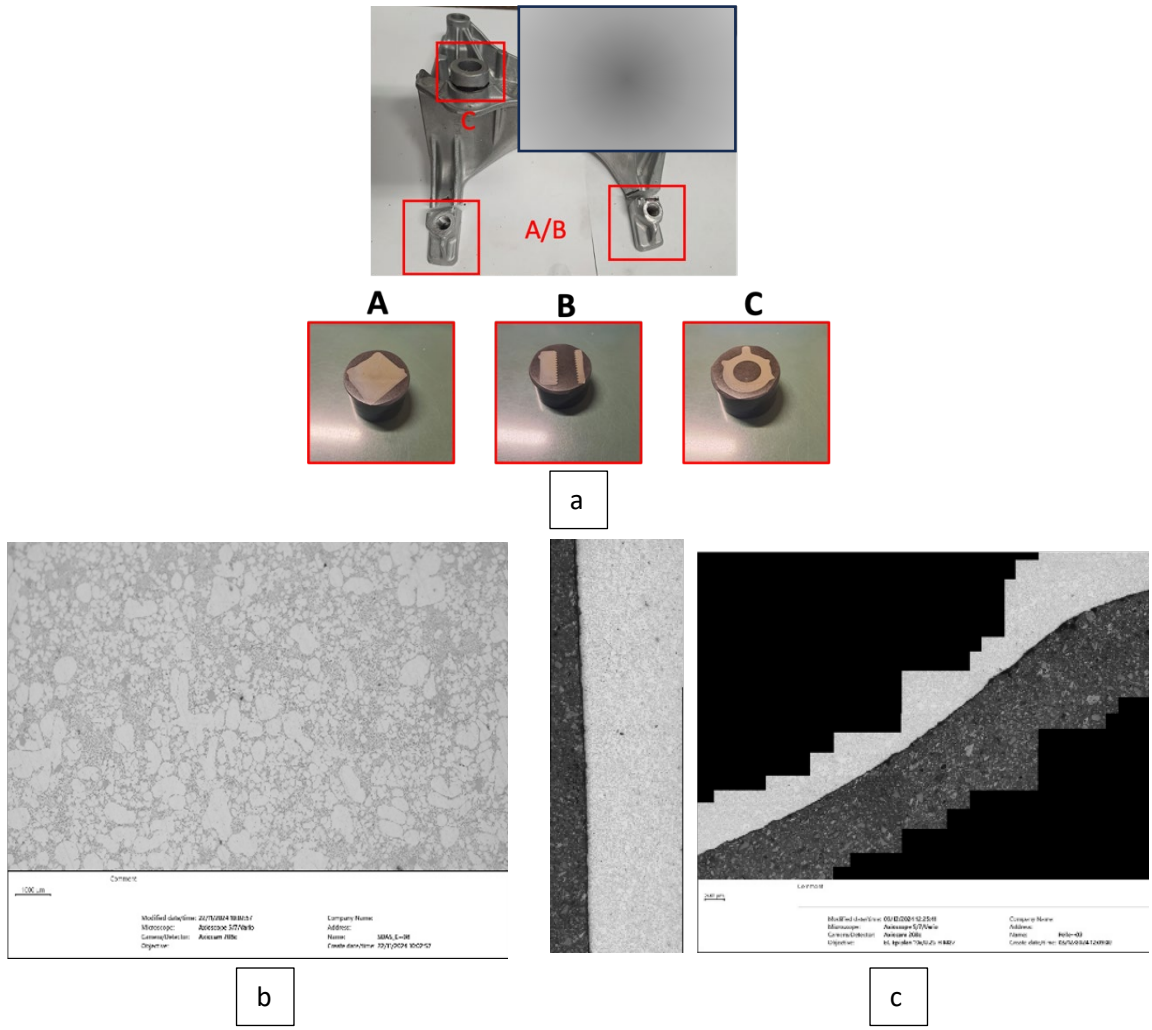


Fig. 8. a) Image of the industrial component, with confidential features intentionally obscured for confidentiality reasons, c)Typical microstructure of the component, b) Skin layer in sections A and C.

Comparison of the Step Casting vs Industrial Component Microstructure

Microstructural analyses were performed on both the step casting specimens and the industrial component with the objective of assessing whether the step casting approach is able to reproduce microstructural features representative of a real, complex HPDC part. The comparison between the industrial component (orange, right-most side bars) and the step casting samples corresponding to the different section thicknesses (blue bars) is summarized in Figure 9 in terms of porosity percentage, SDAS and skin layer thickness. In all graphs, the thin error bars indicate the intrinsic variability of the measured quantities.

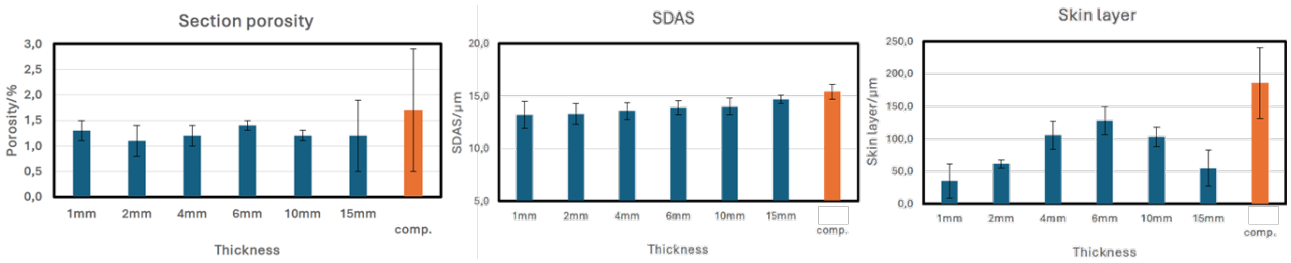


Fig. 9. Comparison of step casting vs industrial component: a) porosity percentage, b) SDAS, c) Skin layer

The porosity results do not show a significant dependence on section thickness, as the measurements were performed at the centre of the steps. Across all investigated sections, including the thicker ones, porosity levels remain low and comparable. This observation is consistent with both ProCAST simulations and X-ray analyses, which indicate that in thicker steps porosity is predominantly localized in the lateral regions rather than in the central area, as a consequence of feeding limitations and local solidification behaviour. The industrial component exhibits a porosity level comparable to the upper range of the step casting values, indicating that the step casting successfully reproduces the defect severity observed in real HPDC parts. The overlap between the variability ranges further supports the representativeness of the step casting geometry. The relatively high scatter observed in the measured porosity is primarily associated with the presence of more massive sections within the industrial component, which exhibit a higher concentration of defects.

However, these regions correspond to low-stress areas of the component and can therefore tolerate such porosity levels without detrimental effects on structural performance. SDAS, instead, slightly increases with increasing section thickness in the step casting, reflecting the reduction in cooling rate. The SDAS measured in the industrial component falls within the range defined by the step casting samples, confirming that the solidification conditions reproduced in the step geometry are consistent with those experienced in the industrial component. This agreement is particularly significant given the complex thermal history and geometry of the real part.

Regarding the skin layer thickness, the step casting results reveal a non-monotonic dependence on section thickness. The skin layer thickness increases with section thickness up to the 6 mm step, beyond which a decrease is observed for thicker sections. This behaviour can be attributed to the combined effect of local cooling rates at the die–metal interface and melt flow conditions during cavity filling. In particular, increased flow turbulence promotes the formation of non-uniform and locally discontinuous skin layers. The industrial component exhibits a skin layer thickness comparable to that measured in the 6mm step casting section and substantially remains within the overall variability envelope defined by the step casting dataset.

Overall, the results demonstrate that the proposed step casting is capable of reproducing not only the average microstructural characteristics of a real HPDC component, but also their inherent spatial variability. This confirms the suitability of the step casting as a reliable experimental benchmark for studying process–microstructure relationships in HPDC and for supporting the validation of numerical simulations and future data-driven modelling approaches.

Conclusion

By integrating numerical modelling with experimental validation, this study provides a practical and reliable framework for linking HPDC process conditions to resulting microstructural properties. The results not only demonstrate the effectiveness of the step casting as a benchmark tool, but also highlight the potential for refining simulation parameters to enhance predictive accuracy. Overall, this work contributes to the broader field of materials and manufacturing science by supporting the development of more robust methodologies, including future analytical and data-driven models, that enable designers to predict the behaviour of lightweight cast components with greater confidence and efficiency.

Fundings

This work was supported by the European Union's Horizon Europe research and innovation programme, Zero Emission electric Vehicles enabled by haRmonised circularity, under No. 101138034.

References

[1] Mielke F, Sulik D, Fang X. Influence of high-pressure die casting parameters on bonding characteristics of aluminium-steel hybrid-castings for automotive lightweight structures. J Manuf Process 2025;143:351–68. https://doi.org/10.1016/J.JMAPRO.2025.04.032.

[2] Graf A. Aluminum alloys for lightweight automotive structures. Materials, Design and Manufacturing for Lightweight Vehicles 2020:97–123. https://doi.org/10.1016/B978-0-12-818712-8.00003-3.

[3] Yang J, Liu B, Shu D, Li H, Yang Q, Hu T, et al. Effect of Casting Pressure on Porosity, Microstructure, and Mechanical Properties of Large Die Casting Aluminum Alloy Parts. International Journal of Metalcasting 2025. https://doi.org/10.1007/S40962-025-01641-4.

[4] Yang W, Puga H, Bolibruchová D, Matejka M, Pastirčák R, Podprocká R. Effect of Piston Velocity on Microstructural Consistency and Critical Regions in a High-Pressure Die Cast AlSi9Cu3(Fe) Alloy Component. Metals 2025, Vol 15, Page 1065 2025;15:1065. https://doi.org/10.3390/MET15101065.

[5] Bonollo F, Gramegna N, Timelli G. High-pressure die-casting: Contradictions and challenges. JOM 2015; 67:901–8. https://doi.org/10.1007/S11837-015-1333-8.

[6] I. Todaro, R. Squatrito, A. Morri, L. Tomesani (2010). Effects of cooling rate on microstructure in EN-AC43000 gravity castings and related T6 mechanical properties. SEATTLE: TMS Light Metals.

[7] Squatrito, Rosario & Todaro, Ivan & Ceschini, Lorella & Morri, Alessandro & Tomesani, Luca. (2011). Hydrogen and cooling rate effetcs on microporosity formation in the production of defect-controlled fatigue specimens. 121-128

[8] Jolly M, Katgerman L. Modelling of defects in aluminium cast products. Prog Mater Sci 2022; 123:100824. https://doi.org/10.1016/J.PMATSCI.2021.100824.

[9] Niklas A. et al, Effect of solution heat treatment on gas porosity and mechanical properties in a die cast step part manufactured with a new AlSi10MnMg(Fe) secondary alloy, http://dx.doi.org/10.1016/j.msea.2016.05.024

[10] Dalai B. et al, Inhomogeneous Skin Formation and Its Effect on the Tensile Behavior of a High Pressure Die Cast Recycled Secondary AlSi10MnMg(Fe) Alloy, https://doi.org/10.1007/s11661-024-07631-1